Supplementary information includes:

Extended Data Figures 1–6

Extended Data Figure legends 1–6

Supplementary Tabels 1 and 2

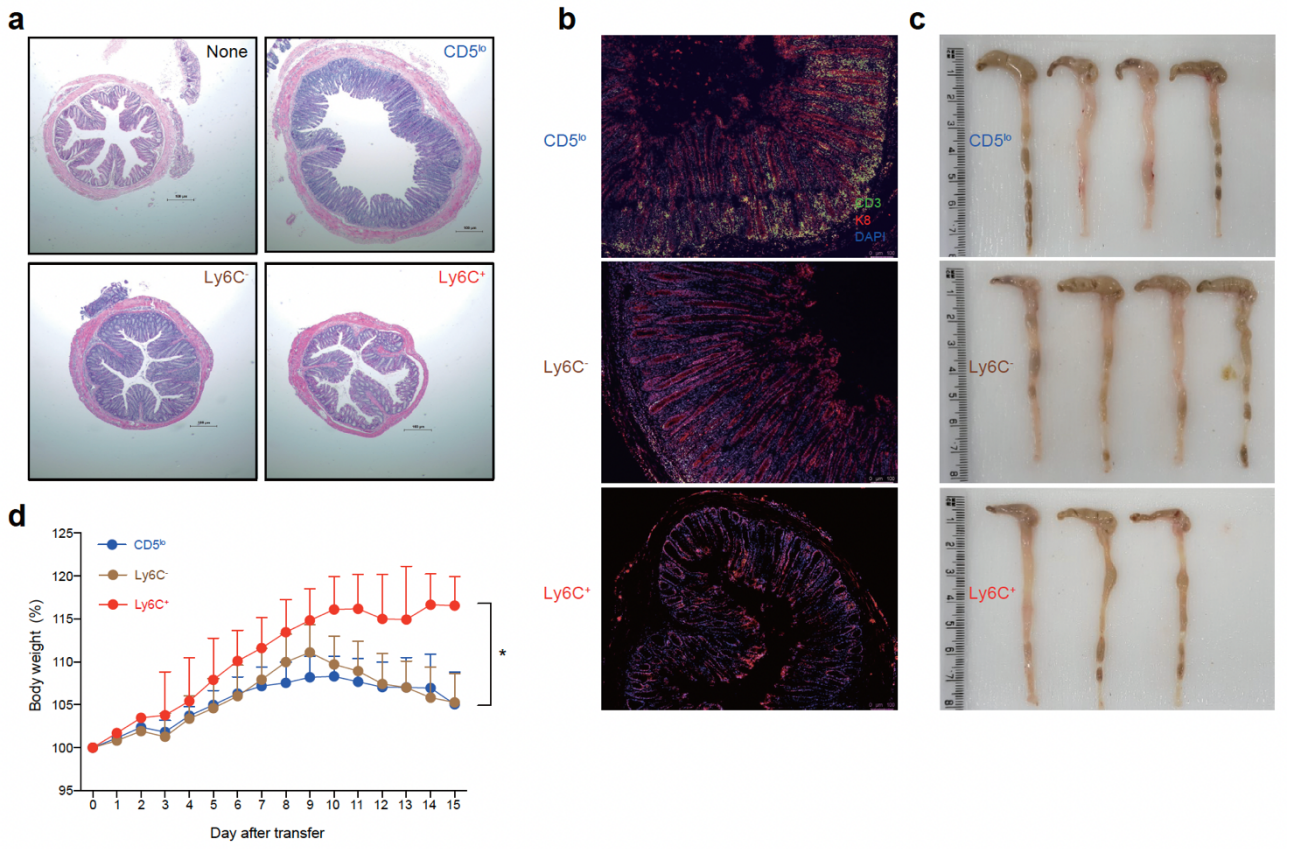

Extended Data Fig. 1. Pathologic symptoms induced by different CD8$^+$ T_N subsets in *Rag1*$^{-/-}$ mice. a–c, Representative H & E staining images **(a**; magnification, 40×), and representative immunofluorescence images **(b**; magnification, 100×), and photo images **(c)** for day 14 LI. **d,** Body weight changes of *Rag1*$^{-/-}$ recipients after adoptive transfer with CD8$^+$ T_N subsets. Data are representative of three **(a–d)** independent experiments (**a–c,** n=3–5; and **d,** n=6 mice/experiment) and presented as the mean ± SD (**d**). Statistical significance by Mann-Whitney test. *, $P < 0.05$; **, $P < 0.01$; ***, $P < 0.001$; ****, $P < 0.0001$.

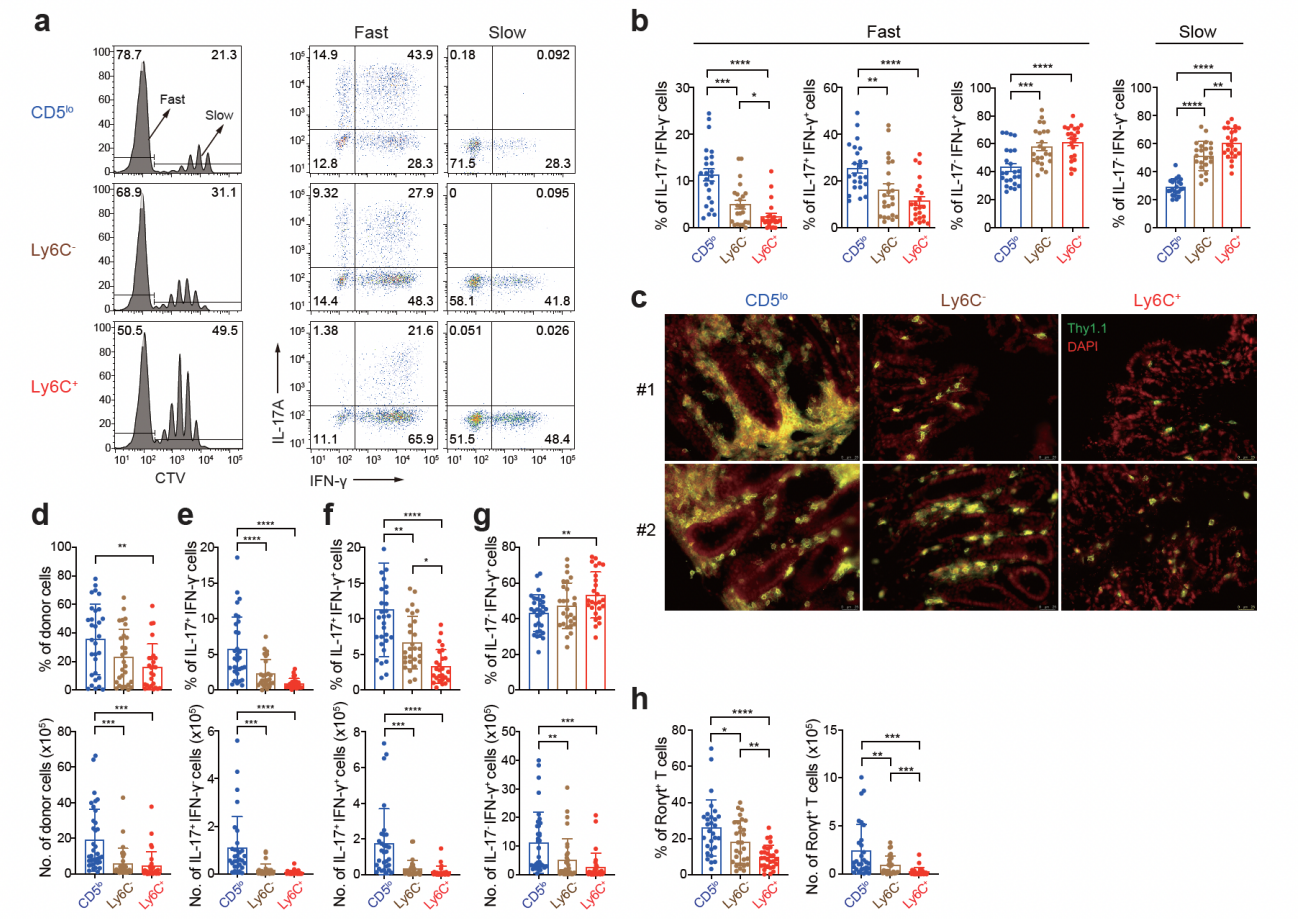

Extended Data Fig. 2. Proliferation, colonic infiltration, and IL-17/IFN-γ production of adoptively transferred CD8$^+$ T$_N$ subsets in *Rag1*$^{-/-}$ mice. a, CTV-labeled CD5^{lo}, Ly6C$^-$, and Ly6C$^+$ CD8$^+$ T$_N$ subsets were adoptively transferred into *Rag1*$^{-/-}$ recipients and the proliferation of donor cells were analyzed at day 7 by measuring CTV dilution. Representative histograms (left) and FACS plots (right) show CTV dilution and IL-17A/IFN-γ production, respectively, for fast and slow proliferative donor cells. **b,** Percentage of IL-17A$^+$IFN-γ$^-$, IL-17A$^+$IFN-γ$^+$, and IL-17A$^-$IFN-γ$^+$ cells for fast (left) and slow (right) proliferative donor subsets in day 7 mLN. **c–h,** Immunofluorescence images for Thy1.1$^+$ donor cells **(c;** magnification, 200×), the percentage and number of total donor **(d)**, IL-17A$^+$IFN-γ$^-$ **(e)**, IL-17A$^+$IFN-γ$^+$ **(f)**, IL-17A$^-$IFN-γ$^+$ **(g)**, and Rorgt$^+$ **(h)** cells from day 14 LI. Data are pooled from three **(b)**, two **(c),** and four **(d–h)** independent experiments (n=6–8 mice/experiment) and presented as the mean ± SEM **(b,d–h)**. Statistical significance by two-way ANOVA Multiple comparisons. *, $P < 0.05$; **, $P < 0.01$; ***, $P < 0.001$; ****, $P < 0.0001$.

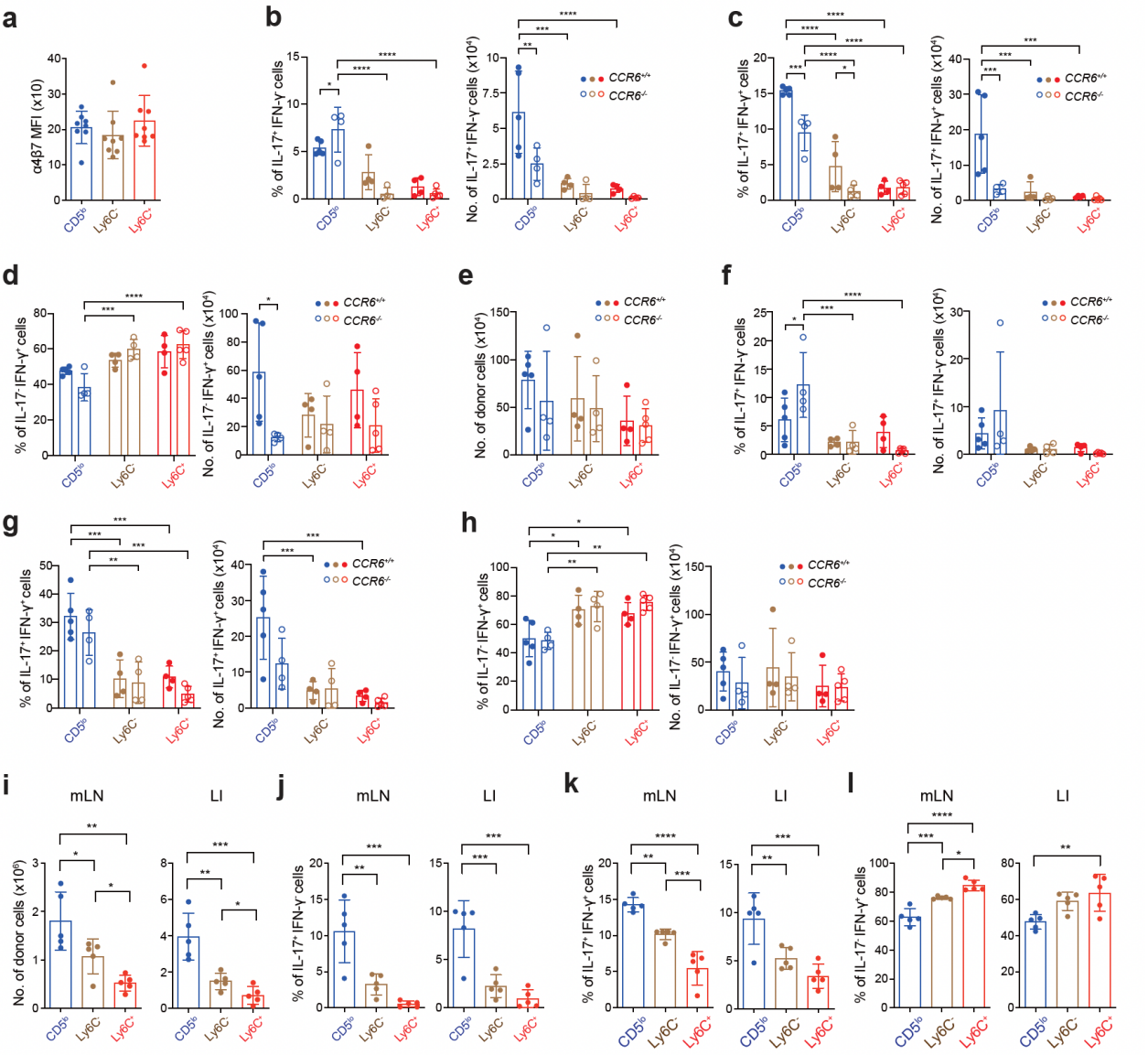

Extended Data Fig. 3. The impact of CCR6 deficiency on IL-17/IFN-γ production of adoptively transferred CD8⁺ T_N subsets in *Rag1*$^{-/-}$ mice. a, Expression levels (MFI) of α4β7 of transferred donor subsets from day 7 mLN. **b–h,** Percentage and number of IL-17A⁺IFN-γ⁻ **(b,f),** IL-17A⁺IFN-γ⁺ **(c,g)**, and IL-17A⁻IFN-γ⁺ **(d,h)** cells, and number of each donor subset **(e)** analyzed in LI (**b–d)** and mLN (**e–h)** at day 14 after adoptive transfer with either *Ccr6*$^{+/+}$ or *Ccr6*$^{-/-}$ CD8⁺ T_N subsets. **i–l,** Number of donor cells **(i)** and the percentage of IL-17A⁺IFN-γ⁻ **(j)**, IL-17A⁺IFN-γ⁺ **(k)**, and IL-17A⁻IFN-γ⁺ **(l)** cells analyzed in LI at day 21 after transfer with *Ccr6*$^{-/-}$ CD8⁺ T_N subsets. Data are representative of two **(a–l)** independent experiments **(a**, n=5–7; **b–d,** n=8–9; **e–h,** n=4–5; and **i–l**, n=5–10 mice/experiment) and presented as the mean ± SD **(a–l)**. Statistical significance by two-way ANOVA Multiple comparisons. *, $P < 0.05$; **, $P < 0.01$; ***, $P < 0.001$; ****, $P < 0.0001$.

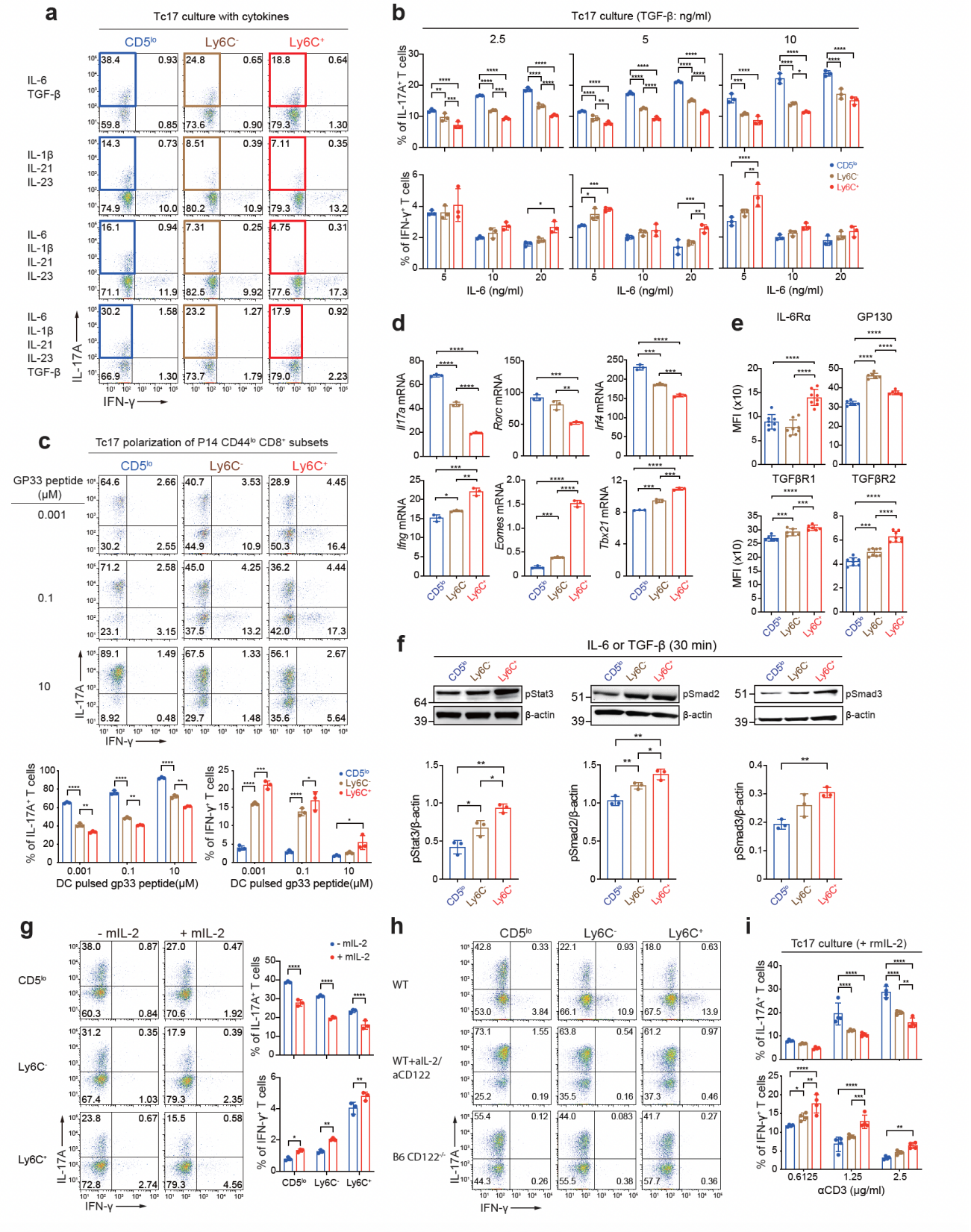

Extended Data Fig. 4. Differential Tc17-skewing potential of CD8$^+$ T_N subsets under various Tc17-polarizing conditions *in vitro*. a, Representative FACS plots for IL-17A/IFN-γ production after

in vitro culture with B6 $CD8^+$ T_N subsets under various Tc17-polarizing conditions. **b,** Percentage of IL-$17A^+$ and IFN-γ^+ cells after Tc17-polarizing culture with B6 $CD8^+$ T_N subsets in the presence of various concentrations of IL-6 and TGF-β. **c,** Representative FACS plots for IL-17A/IFN-γ production from P14 $CD8^+$ T_N subsets stimulated with GP33 peptide-pulsed dendritic cells under Tc17-polarizing condition. **d,** qRT-PCR data for *Il17a, Rorc,, Irf4, Ifng*, *Eomes,* and *Tbx21* after Tc17-polarizing culture with B6 $CD8^+$ T_N subsets. **e,** Expression levels (MFI) of IL-6Rα, GP130, TGFβRI, and TGFβRII on B6 $CD8^+$ T_N subsets (n=6–8 mice/group). **f,** Levels of p-STAT3, p-SMAD2, and p-SMAD3 (shown in representative blot images, top, and intensity relative to β-actin, bottom). **g,** Representative FACS plots for IL-17A/IFN-γ production (left) and the percentage of IL-$17A^+$ and IFN- γ^+ cells (right) after Tc17-polarizing culture with B6 $CD8^+$ T_N subsets in the presence or absence of rmIL-2. **h,** Representative FACS plots for IL-17A/IFN-γ production after Tc17-polarizing culture with B6 $CD8^+$ T_N subsets in the presence (middle) or absence (top) of anti-IL-2/CD122 or with *Cd122*$^{-/-}$ $CD8^+$ T_N subsets (bottom). **i,** Percentage of IL-$17A^+$ and IFN-γ^+ cells after Tc17-polarizing culture of B6 $CD8^+$ T_N subsets with various concentrations of anti-CD3 and rmIL-2. Data is representative of two to three independent experiments (**a–i)** and presented as the mean ± SD **(b–g,i)**. Statistical significance by two-way ANOVA Multiple comparisons. *, $P < 0.05$; **, $P < 0.01$; ***, $P < 0.001$; ****, $P < 0.0001$.

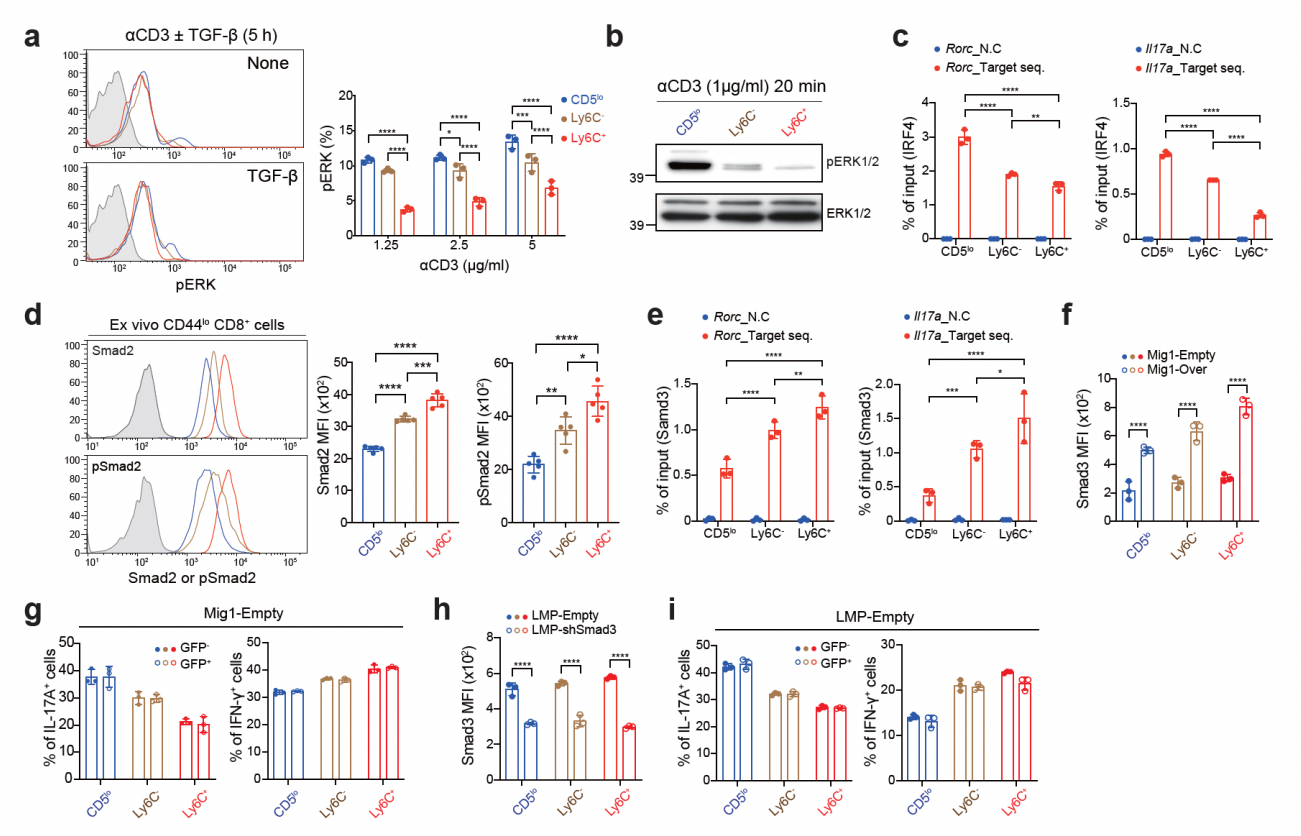

Extended Data Fig. 5. Differential levels of TCR-induced ERK activation and endogenous SMAD2 expression in CD8$^+$ T$_N$ subsets. a, Histogram (left) and percentage (right) for p-ERK expression among CD8$^+$ T$_N$ subsets stimulated with either anti-CD3 in the presence or absence of TGF-β (left) or with various concentrations of anti-CD3 (right). **b,** Representative blot images of p-ERK after 20 min stimulation with anti-CD3. **c,** B6 CD8$^+$ T$_N$ subsets were activated under Tc17-polarizing conditions for 72 h and subjected to ChIP using IRF4 antibody. Eluted DNA was analyzed by qPCR. **d,** Endogenous levels of SMAD2 and p-SMAD2 in *ex vivo* B6 CD8$^+$ T$_N$ subsets shown in histogram (left) and MFI (right) (n=5 mice/group). **e,** B6 CD8$^+$ T$_N$ subsets were activated under Tc17-polarizing conditions for 72 h and subjected to ChIP using SMAD3 antibody. Eluted DNA was analyzed by qPCR. **f,** MFI levels of SMAD3 from Tc17-polarized CD8$^+$ T$_N$ subsets transduced with either MigR-1 control (empty) or MigR-1 vector encoding *SMAD3* (over). **g,** Percentage of IL-17A$^+$ and IFN-γ$^+$ cells in GFP$^-$ and GFP$^+$ cells transduced with MigR-1 empty vector control. **h,** MFI levels of SMAD3 for Tc17-polarized CD8$^+$ T$_N$ subsets transduced with either LMP empty vector control or LMP vector containing *SMAD3* shRNA. **i,** Percentage of IL-17A$^+$ and IFN-γ$^+$ cells in GFP$^-$ or GFP$^+$ cells transduced with LMP empty vector control. Data are representative of two to three independent experiments **(a–i)** and presented as the mean ± SD **(a,c–i)**. Statistical significance by two-way ANOVA Multiple comparisons. *, $P < 0.05$; **, $P < 0.01$; ***, $P < 0.001$; ****, $P < 0.0001$.

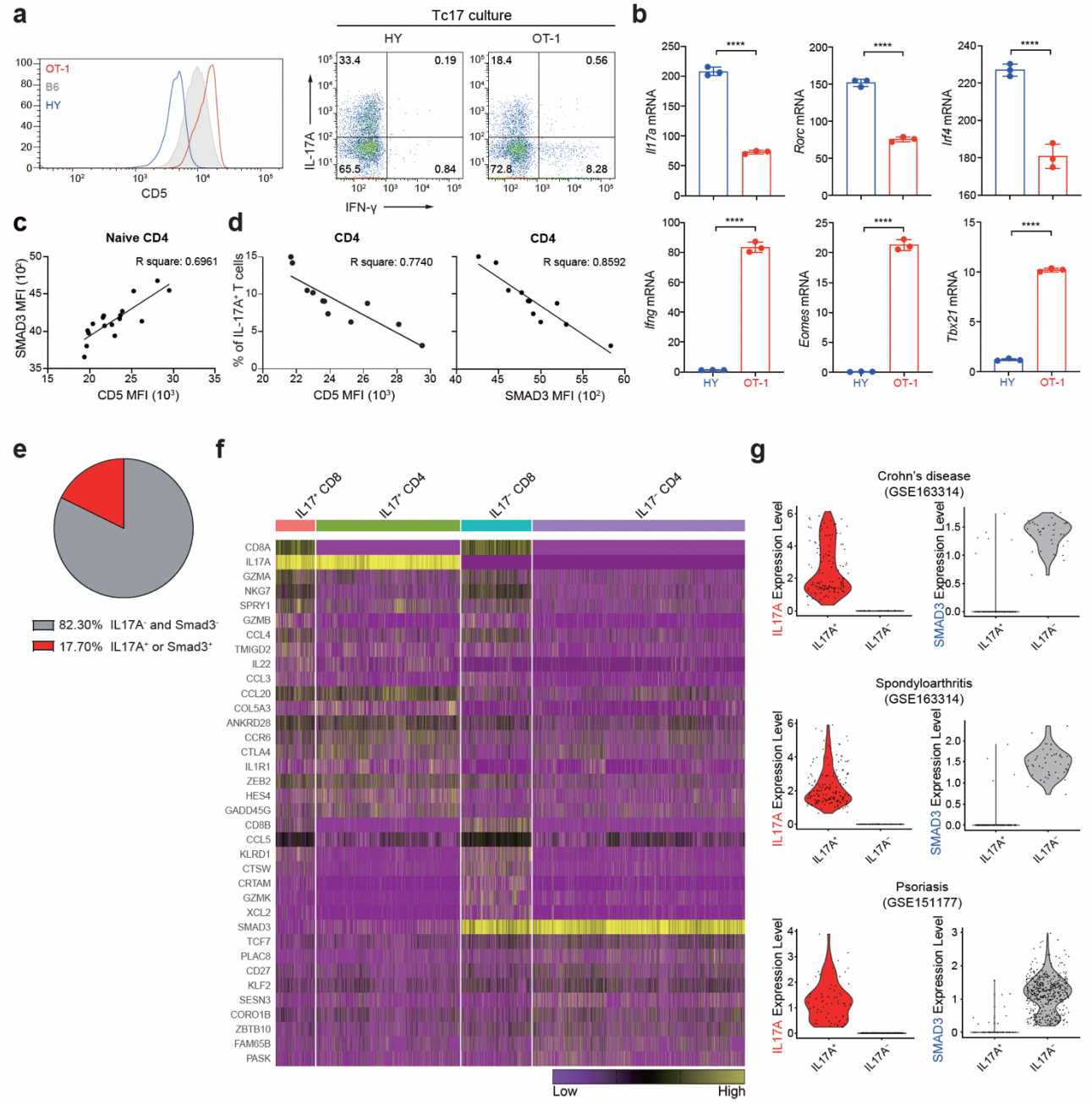

Extended Data Fig. 6. Inverse relationship between CD5 and SMAD3 expression and Tc17 differentiation potential in mice and humans. a, Expression levels of CD5 shown in histogram for HY and OT-1 *ex vivo* (left), and representative FACS plots for IL-17A/IFN-γ production (right) after Tc17-polarizing culture. **b,** qRT-PCR data for *Il17a, Rorc, Irf4, Ifng, Eomes,* and *Tbx21* analyzed for Tc17-polarized HY and OT-1 CD8$^+$ T_N cells. **c,** Relationship between CD5 and SMAD3 levels *ex vivo* in CD4$^+$ T_N populations from healthy human PBMC (n=17). **d,** Relationship between CD5 (left) or SMAD3 (right) levels *ex vivo* and the percentages of IL-17A$^+$ cells after Th17-polarizing cultures with human CD4$^+$ T_N populations (n=11). **e,f,** *IL17A* and *SMAD3* expression profiles in *CD3*$^+$ cells **(e)** and

heatmap of differentially expressed genes of *IL17*$^{+}$*CD8*$^{+}$, *IL17*$^{+}$*CD4*$^{+}$, *IL-17*$^{-}$*CD8*$^{+}$, and *IL17*$^{-}$*CD4*$^{+}$ T cells **(f)** in public single cell RNA-sequencing (scRNA-seq) data set (GSE162335) performed with patients' tissues (lamina propria) with UC. **g,** *IL17A* and *SMAD3* expression of *CD3*$^{+}$ cells that are either *IL17A*$^{+}$ or *SMAD3*$^{+}$ in public scRNA-seq data sets (GSE162335, GSE163314, and GSE151177) performed with tissues from patients with Crohn's disease, Spondyloarthritis, and Psoriasis, respectively. Data are representative **(a,b)** or pooled **(c,d)** from two to three independent experiments and presented as the mean ± SD **(d)**. Statistical significance by simple linear regression two-way ANOVA Multiple comparisons. *, $P < 0.05$; **, $P < 0.01$; ***, $P < 0.001$; ****, $P < 0.0001$.

Supplementary Table 1.

Antibodies	Manufacturer	Catalog #
anti-CD16/32	ebioscience	14-0161-82
anti-Vβ2 (FITC); clone B20.6	Biolegend	127906
anti-Vβ3 (FITC); clone KJ25	BD Bioscience	553208
anti-Vβ4 (FITC); clone KT4	BD Bioscience	553365
anti-Vβ5.1/5.2 (FITC); clone MR9-4	ThermoFisher	11-5796-80
anti-Vβ6 (FITC); clone RR4-7	BD Bioscience	553193
anti-Vβ7 (FITC); clone TR310	Biolegend	118306
anti-Vβ8.3 (FITC); clone 1B3.3	BD Bioscience	553663
anti-Vβ9 (FITC); clone MR10-2	BD Bioscience	553201
anti-Vβ10b (FITC); clone B21.5	BD Bioscience	553284
anti-Vβ11 (FITC); clone RR3-15	BD Bioscience	553197
anti-Vβ12 (FITC); clone MR11-1	BD Bioscience	553300
anti-Vβ13 (FITC); clone MR12-3	BD Bioscience	553204
anti-Vβ14 (FITC); clone 14-2	BD Bioscience	553258
anti-Vβ17a (FITC); clone KJ23	BD Bioscience	553212
anti-CD3ε (PB); clone 145-2C11	Biolegend	100334
anti-CD5 (PE); clone 53-7.3	Invitrogen	12-0051-83
anti-CD44 (eF450); clone IM7	Invitrogen	48-0441-82
anti-CD62L (PE); clone MEL-14	Biolegend	104408
anti-CD45.1 (BUV395); clone A20	BD Bioscience	565212
anti-CD45.2 (PB); clone 104	Biolegend	109820
anti-CD90.1 (FITC); clone HIS51	Invitrogen	11-0900-85
anti-CD90.2 (PE) (53-2.1)	ebioscience	15298609
anti-Ly6C (PE-cy7) (HK1.4)	ebioscience	15518606
anti-CD8α (APC) (53-6.7)	Tonbo	20-0081-U100
anti-CD126 (APC) (D7715A7)	Biolegend	115812
anti-GP130 (APC); clone KGP130	ThermoFisher	17-1302-82
anti-TGFBRI (APC); clone 141231	R&D biosystems	FAB5871A
anti-TGFBRII (PE); polyclonal	R&D biosystems	FAB532P
anti-α4β7 (APC); clone DATK32	ThermoFisher	17-5887-82
anti-CD195 (PE); clone HM-CCR5	ebioscience	12-1951-81
anti-CD196 (PE); clone 29-2L17	Biolegend	129804
anti-IFN-γ (APC); clone XMG1.2	Invitrogen	17-7311-82
anti-IL-17A (PE); clone eBio17B7	Invitrogen	12-7177-81
anti-Eomes (APC)	ebioscience	50-4875-82
anti-Rorgt (PE); clone B2D	Invitrogen	12-6981-82
anti-Rorgt (PE-eF610); clone B2D	Invitrogen	61-6981-82
anti-IRF4 (APC); clone IRF4.3E4	Biolegend	646408
anti-GM-CSF (PE); clone MP1-22E9	Invitrogen	12-7331-82
anti-pERK (PE); clone py204	BD Bioscience	612566
anti-hCD3 (APC-cy7); clone HIT3a	Biolegend	300318
anti-hCD4 (APC); clone A161A1	Biolegend	357408
anti-hCD5 (PE); clone L17F12	Biolegend	364014
anti-hCD8 (FITC); clone SK1	Biolegend	344704
anti-hCD45RA (PB); clone HI100	Biolegend	304123
anti-hCCR7 (PE-cy7); clone G043H7	Biolegend	353225
anti-hIFN-γ (APC); clone B27	Biolegend	506510
anti-hIL-17A (PE); clone BL168	Biolegend	512306

Supplementary Table 2.

Rorc region (IRF4)	Sense primer	Antisense primer
N.C_-1576 ~ -1737	TGAGCACACTATCACTCTCTTCAG	TGACCCTTGGGTAGGAGAGA
Target_+10747 ~ +10824	GGGCCCTGAGATGGTAAGTT	GGGTGCTGAGTAATCACAGGA

Il17a region (IRF4)	Sense primer	Antisense primer
N.C_-3387 ~ -3523	CTCCCATGTGGTCATTATTGC	GTGTCCTTAGGTCCTAAATGTAGG
Target_-1592~-1815	AATCCATGGAGCTGGAGAGA	TTTTTATACAACATAGGTCTTCATGG

Rorc region (Smad3)	Sense primer	Antisense primer
N.C_-727 ~ -881	GGTTGTTGGGTAAGCAGGAA	CACGACCCCGTAATTCTGTT
Target_-862 ~ -1181	CAACGGTGGAGAATGGAATG	TTCCTGCTTACCCAACAACC

Il17a region (Smad3)	Sense primer	Antisense primer
N.C_-1211 ~ -984	CAGGGATAATGCCAAGGGTA	AGCATGAGGTGGACCGATAG
Target_-11~ -185	AACTTCTGCCCTTCCCATCT	GCTCCTTTCTCTCTTTTTATACGG

Smad3 overexpression	
Forward	GACTCGAGATGTCGTCCATCCTGCCC
Reverse	GAGAATTCCTAAGACACACTTTAACAGCG

shRNA sequence for Smad3	TGCTGTTGACAGTGAGCGAACGCAGAACGTGAACACCAAGTAG TGAAGCCACAGATGTACTTGGTGTTCACGTTCTGCGTGTGCCTAC